

## Luminescence of Europium(III) and Manganese(II) in Barium and Zinc Orthosilicate

Ana Maria Pires and Marian Rosaly Davolos\*

Instituto de Química, UNESP, P.O. Box 355, 14801-970, Araraquara, SP, Brazil

Received January 24, 2000. Revised Manuscript Received September 25, 2000

The aim of this work is to report on the luminescence properties of  $\text{BaZnSiO}_4$  activated by  $\text{Eu}^{3+}$  and  $\text{Mn}^{2+}$  ions. Doped and undoped powder samples were prepared by solid-state reaction starting from oxides and carbonates or  $\text{Ba}_2\text{SiO}_4\cdot\text{Eu}^{3+}$  and  $\text{Zn}_2\text{SiO}_4\cdot\text{Mn}^{2+}$  precursors. X-ray diffraction powder data, IR vibrational, and UV–vis luminescence spectroscopies were carried out. Results showed that doped and undoped samples from both types of precursors have the same structure and crystallize with a superstructure of hexagonal kalsilite. Vibrational spectroscopy has confirmed the formation of a silicate group, which outlines differences between products and silicate precursors. The observed luminescence assigned to  $\text{Eu}^{3+}$  and  $\text{Mn}^{2+}$  transitions covered most parts of the visible spectrum, an important requirement for phosphors in fluorescent low-pressure mercury vapor lamps.

### Introduction

Phosphors or luminescent materials are widely used to generate visible light, mainly in a fluorescent lamp field. There are two kinds of fluorescent lamps to generate white light: high- and low-pressure mercury vapor lamps.<sup>1</sup> Basically, both lamps require phosphors that absorb UV radiation and emit an appropriate color set that results in white emission. Among the host lattices for luminescent materials, specially the ones used in lamps,<sup>2</sup> silicate compounds have been extensively investigated<sup>3–8</sup> because of their stability, visible light transparency, and relative easy preparation. For instance, zinc orthosilicate (willemite,  $\text{Zn}_2\text{SiO}_4$ , trigonal crystalline system,  $\bar{R}3$  space group<sup>3</sup>) doped with divalent manganese ions is commercially used as a green phosphor, which has been studied by various experimental techniques since the 1930s.<sup>4</sup> Other luminescent colors can be achieved by using  $\text{Eu}^{2+}$  in  $\text{Ba}_2\text{SiO}_4$ ,<sup>5</sup>  $(\text{Ca},\text{Sr})_2\text{MgSi}_2\text{O}_7$ ,  $\text{MSiO}_3$  ( $M = \text{Ba}, \text{Sr}, \text{Ca}$ ),  $\text{BaSi}_2\text{O}_5$ ,  $\text{BaMgSiO}_4$ ,  $\text{CaMgSiO}_4$ , and  $\text{Sr}_2\text{LiSiO}_4\text{F}$ .<sup>6</sup> Recently, the matrix  $\text{Ba}_2\text{SiO}_4$  (orthorhombic crystal system,  $Pm\bar{c}n$

space group) was doped with  $\text{Eu}^{3+}$  ion and was reported as a red phosphor presenting anomalous  $\text{Eu}^{3+}$  transitions.<sup>7</sup> Also, it was shown that  $\text{Mn}^{5+}$  can be stabilized in this matrix of  $\text{Ba}_2\text{SiO}_4$ .<sup>8</sup>

A tricolor lamp is a type of low-pressure vapor lamp obtained by combining three phosphors that emit light in narrow wavelength intervals centered at around 450, 550, and 610 nm.<sup>9</sup> In this context, one host lattice that can be activated by different ions emitting in different regions of the visible spectrum is a challenge for the solid materials syntheses. It is important to find a matrix in which different activation ions can be structurally substituted for cation sites.  $\text{BaZnSiO}_4$ , whose structure has already been investigated,<sup>10–12</sup> may incorporate different doping ions and has not been studied as a matrix for luminescent materials so far. The aim of this work is to report on luminescent properties of  $\text{BaZnSiO}_4$  activated by  $\text{Eu}^{3+}$  and  $\text{Mn}^{2+}$  ions for application feasibility in a fluorescent lamp field.

### Experimental Section

**Sample Preparation.**  $\text{BaZnSiO}_4$  doped with  $\text{Eu}^{3+}$  and  $\text{Mn}^{2+}$  (both 2 at. %) and undoped powder samples were prepared by a solid-state reaction, using a tubular furnace with alumina tubes and boats at 1200 °C for 12 h under a dynamic argon atmosphere. To obtain an X-ray powder data pattern,

\* To whom correspondence should be addressed. E-mail: davolos@helio.iq.unesp.br.

- (1) Welker, T. J. *J. Luminesc.* **1991**, *48/49*, 49.
- (2) Butler, K. H. *Fluorescent Lamp Phosphors*; The Pennsylvania State University Press: University Park, PA, 1980.
- (3) Klaska, K. H.; Eck, J. C. D. Pohl, *Acta Crystallogr.* **1978**, *B34*, 3324.
- (4) Mishra, K. C.; Johnson, K. H.; Deboer, B. G.; Berkowitz, J. K.; Olsen, J.; Dale, E. A. *J. Luminesc.* **1991**, *47*, 197.
- (5) Barry, T. L. *J. Electrochem. Soc.* **1968**, *115*, 1181.
- (6) Poort, S. H. M.; Reijnhoudt, H. M.; Van Der Kuip, H. O. T.; Blasse, G. *J. Alloys Compd.* **1996**, *241*, 75.
- (7) Pires, A. M.; Davolos, M. R.; Malta, O. L. *J. Luminesc.* **1997**, *72–74*, 244.
- (8) Ferracin, L. C.; Davolos, M. R.; Nunes, L. A. O. *J. Luminesc.* **1997**, *72–74*, 185.

(9) Blasse, G.; Grabmaier, B. C. *Luminescent Materials*; Springer-Verlag: New York, 1994.

(10) Do Dinh, P. C.; Durif, A. *Bull. Soc. Fr. Minér. Cristallogr.* **1964**, *87*, 108.

(11) Powder Diffraction File PDF-2 database sets 1–44. Pennsylvania Joint Committee on Powder Diffraction Standards–International Center for Diffraction Data. c 1988, PDG number 42-0335. (CD-ROM). Ref: Manke, A.; Eysel, W. *Mineral-Petrograph*; Institut Der Universitaet Heidelberg: Germany, Iced Grant-In-Aid, 1991.

(12) Liu, B.; Barbier, J. J. *Solid State Chem.* **1993**, *102*, 115.

the undoped BaZnSiO<sub>4</sub> sample was heated twice, resulting in 36 h of total heating time. The starting materials used for the undoped powder were Ba<sub>2</sub>SiO<sub>4</sub> and Zn<sub>2</sub>SiO<sub>4</sub>, independently prepared from BaCO<sub>3</sub> (Merck), ZnO (Baker & Adams), and SiO<sub>2</sub> (Merck, 60 HR), all grade reagents, at 1200 °C for 4 h in an argon dynamic flow. Oxygen, water vapor, and carbon dioxide impurities were avoided during dynamic argon flow by using an adequate purifying system. The doped samples were obtained by two methods: Method 1 (M1)—starting from previously obtained doped orthosilicates (Ba<sub>2</sub>SiO<sub>4</sub>:Eu<sup>3+</sup> and Zn<sub>2</sub>SiO<sub>4</sub>:Mn<sup>2+</sup>). Method 2 (M2)—using a stoichiometric mixture containing the oxides and carbonate and the activators, Eu<sub>2</sub>O<sub>3</sub> (Aldrich, 99.99%) and MnCO<sub>3</sub> (Riedel), homogenized by grinding the powders in mortar agate. The experimental conditions (time, temperature, and atmosphere) in both methods and in the undoped compound preparation were the same. The doped sample prepared by method 1, M1, was annealed as well as the other sample prepared by method 2, M2, resulting in 24 h of total heating time.

**Sample Characterization.** In all cases, the structure of the powders was checked by X-ray powder diffraction using a Siemens D5000 diffractometer ( $\Delta 2\theta = 4^\circ - 70^\circ$ ,  $0.2^\circ$  increments, integration time = 3 s, Cu K $\alpha_1$  radiation,  $\lambda = 1.540598 \text{ \AA}$ , and secondary graphite monochromator). The compounds were also checked by IR vibrational absorption spectroscopy (infrared spectrophotometer Nicolet, model FT-IR 730). Excitation and emission spectra were recorded using a Fluorolog SPEX F2121 spectrofluorimeter equipped with a 450-W xenon lamp as the light source and Hamamatsu R928 photomultiplier. Lifetime measurements were carried out with a 1934 phosphorimeter coupled with the spectrofluorimeter and equipped with a pulsed xenon lamp EG&GFX-265.

## Results and Discussion

**1. X-ray Diffraction Powder Data.** X-ray diffractograms obtained for all samples are represented in Figure 1. The undoped sample X-ray diffractogram was also analyzed using Rietveld refinements performed by the DBWS-9411<sup>13</sup> program to compare with literature results. The unit-cell parameters calculated as well as literature values reported by different references and summarized in the next paragraph are listed in Table 1.

Initially, Ba-substituted BaAl<sub>2</sub>O<sub>4</sub> compounds, BaZn-GeO<sub>4</sub>, BaMgSiO<sub>4</sub>, and BaZnSiO<sub>4</sub>, were reported by Do Dinh and Durif<sup>10</sup> as crystallizing with small hexagonal unit cells, suggesting that they were isostructural with kalsilite (KAlSiO<sub>4</sub>). Diffraction powder data about the BaZnSiO<sub>4</sub> structure were reported in JCPDS-International Centre for Diffraction<sup>11</sup> in agreement with Do Dinh and Durif.<sup>10</sup> However, other studies established the existence of a ( $2 \times A, C$ ) superstructure for BaAl<sub>2</sub>O<sub>4</sub><sup>14</sup> and a temperature-dependent ( $\sqrt{3} \times A, 4 \times C$ ) superstructure for BaZnGeO<sub>4</sub>.<sup>15-17</sup> BaMgSiO<sub>4</sub> and BaZnSiO<sub>4</sub> compounds were also reinvestigated using powder X-ray and neutron diffractions, and the discovering of a new isostructural compound, BaCoSiO<sub>4</sub>, was reported by Liu and Barbier.<sup>12</sup> Those authors refined the crystal structures of BaMSiO<sub>4</sub> (M = Co, Mg, and Zn) compounds and showed that they are isostructural Ba-stuffed derivatives of tridymite (SiO<sub>2</sub>) and crystallize with a

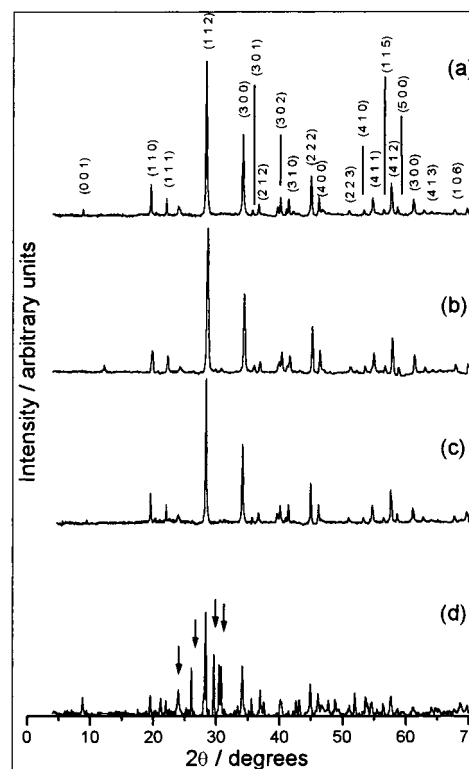


**Figure 1.** Powder X-ray diffractogram of (a) BaZnSiO<sub>4</sub> undoped sample obtained after solid state reaction under 1200 °C for 36 total heating hours. (b) BaZnSiO<sub>4</sub>:Eu<sup>3+</sup>,Mn<sup>2+</sup> sample obtained from a mixture containing the oxides and carbonates (M2) with 12 total heating hours. (c) BaZnSiO<sub>4</sub>:Eu<sup>3+</sup>,Mn<sup>2+</sup> sample obtained from a mixture containing the oxides and carbonates (M2) with 24 total heating hours. (d) BaZnSiO<sub>4</sub>:Eu<sup>3+</sup>,Mn<sup>2+</sup> sample obtained from Ba<sub>2</sub>SiO<sub>4</sub>:Eu<sup>3+</sup> and Zn<sub>2</sub>SiO<sub>4</sub>:Mn<sup>2+</sup> (M1) with 12 total heating hours. The *hkl* reflections were assigned according to mathematical simulation using unit-cell parameters from ref 12.

**Table 1. Hexagonal Unit-Cell Parameters (Å) and Volumes (Å<sup>3</sup>) for BaZnSiO<sub>4</sub>**

BaZnSiO <sub>4</sub>	<i>a</i>	<i>c</i>	<i>V</i>	space group
ref 10	5.244(3)	8.735(5)	104.0	<i>P</i> <sub>6</sub> <sub>3</sub> 22
ref 11	5.2518(3)	8.729(1)	208.50	<i>P</i> <sub>6</sub> <sub>3</sub> 22
ref 12	9.0955(5)	8.7251(9)	625.11(7)	<i>P</i> <sub>6</sub> <sub>3</sub>
undoped sample (36 h)	9.1005	8.7314	626.36	

( $\sqrt{3} \times A, C$ ) superstructure of hexagonal (*A, C*) kalsilite (KAlSiO<sub>4</sub>). The structure refinements reported allowed the determination of the atomic positions and the *P*<sub>6</sub><sub>3</sub> space group for the isostructural subcell of the BaZnGeO<sub>4</sub> compound. Three Ba atoms positioned on the *2a* and *2b* sites and the Si, O, Mg, or Zn atoms occupying three sets of general *6c* sites were identified. Two Ba sites presented a coordination number, CN, of 9 (*2a* and *2b* sites), the third had a CN of 6 (*2b* site), and the Zn site had a CN of 4.

The unit-cell parameters listed in Table 1 show that there is good agreement between the literature and the prepared BaZnSiO<sub>4</sub> undoped sample (36 h total heating time) values, suggesting that the method starting from the silicates is successfully applied here. In the literature, the preparation of BaZnSiO<sub>4</sub> was carried out by high-temperature sintering at 1300 °C for about 48–72 h of a mixture containing Ba(CH<sub>3</sub>COO)<sub>2</sub>, ZnO, and silica gel.<sup>12</sup> The purpose in this work of using silicates

(13) Young, R. A. *J. Appl. Crystallogr.* **1995**, *28*, 366–7.

(14) Hörkner, W.; Müller-Buschbaum, Hk. *Z. Z. Anorg. Allg. Chem.* **1979**, *40*, 475.

(15) Takei, H.; Tsunekawa, S.; Maeda, M. *J. Mater. Sci.* **1980**, *15*, 2612.

(16) Takei, H. *J. Appl. Crystallogr.* **1980**, *13*, 400.

(17) Iijima, K.; Marumo, F.; Takei, H. *Acta Crystallogr.* **1982**, *B38*, 1112.

Table 2. Ionic Radii Difference Percentage between Matrix and Doping Ions<sup>a</sup>

compd	dopant	radii/pm (CN) <sup>19</sup>	difference % between ionic radii			ion-oxygen average distance/pm
			Ba1 166(10)	Ba2 161(9)	Si 40(4)	
Ba <sub>2</sub> SiO <sub>4</sub>	Eu <sup>2+</sup>	149(10)	10.2			
	Eu <sup>2+</sup>	144(9)		10.6	-260	
	Eu <sup>3+</sup>	126(9)	24.1	21.7		
	Eu <sup>3+</sup>	121(8)	27.3	25.1		Ba1-O 298.3
	Mn <sup>2+</sup>	110(8)	33.7	31.7		
	Mn <sup>2+</sup>	80(4hs)			-100	Ba2-O 282.4
	Mn <sup>3+</sup>	78.5(6hs)	52.7	51.2		
	Mn <sup>3+</sup>	72.0(5)			-80	Si-O 163.2
	Mn <sup>4+</sup>	67.0(6)	59.6	58.4		
	Mn <sup>4+</sup>	53.0(4)			-32.5	
	Mn <sup>5+</sup>	47.0(5)	71.7	70.8		
	Mn <sup>5+</sup>	47.0(4)			-17.5	
	Mn <sup>6+</sup>	39.5(4)	72.2	75.5	-1.25	
	Mn <sup>7+</sup>	39.0(4)	76.5	75.8	-2.50	

compd	dopant	radii/pm (CN) <sup>19</sup>	difference % between ionic radii		ion-oxygen average distance/pm
			Zn 74(4)		
Zn <sub>2</sub> SiO <sub>4</sub>					Zn1-O 194.95
	Eu <sup>2+</sup>	131(6)	-77.0		Zn2-O 196.13
	Eu <sup>3+</sup>	109(6)	-46.9		Si-O 163.45
	Mn <sup>2+</sup>	80.0(4hs)	-8.11		O-O 266.83 (tetr.Si)
	Mn <sup>3+</sup>	72.0(5)	2.70		O-O 317.93 (tetr.Zn1)
	Mn <sup>4+</sup>	53(4)	28.38		O-O 319.98 (tetr.Zn2)
	Mn <sup>5+</sup>	47.0(4)	36.49		Si-Zn(1) 311.2
	Mn <sup>6+</sup>	39.5(4)	53.38		Si-Zn(2) 309.4
	Mn <sup>7+</sup>	39.0(4)	47.30		Zn1-Zn2 311.2

compd	dopant	radii/pm (CN) <sup>19</sup>	difference % between ionic radii			ion-oxygen average distance/pm
			Ba1&2 61(9)	Ba3 149(6)	Zn 74(4)	
BaZnSiO <sub>4</sub>	Eu <sup>2+</sup>	144(9)	10.6		-94.6	
	Eu <sup>2+</sup>	131(6)		12.08	-77.0	
	Eu <sup>3+</sup>	126(9)	21.74		-70.3	Ba1-O 288.0
	Eu <sup>3+</sup>	109(6)		27.05	-46.9	
	Mn <sup>2+</sup>	110(8)	31.67			Ba[2]-O 294.0
	Mn <sup>2+</sup>	81.0(6ls)		45.64		
	Mn <sup>2+</sup>	97.0(6hs)		34.9		Ba[3]-O 272.0
	Mn <sup>2+</sup>	80.0(4hs)			-8.11	
	Mn <sup>3+</sup>	72.0(6ls)		51.68	2.70	Si-O 163.0
	Mn <sup>3+</sup>	78.5(6hs)		47.31		
	Mn <sup>4+</sup>	53.0(4)		64.4	28.3	Zn-O 192
	Mn <sup>4+</sup>	67.0(6)		55.0		
	Mn <sup>5+</sup>	47.0(5)		68.5	36.5	
	Mn <sup>6+</sup>	39.5(4)		73.5	46.6	
	Mn <sup>7+</sup>	39.0(4)		73.8	47.3	

<sup>a</sup> CN = coordination number; hs = high spin; ls = low spin.

as precursors is to supply already formed silica tetrahedrons during their reaction to decrease time and temperature reaction. On the basis of the structure of BaCoSiO<sub>4</sub> reported by Liu and Barbier,<sup>12</sup> the structure of BaZnSiO<sub>4</sub> viewed along the *c* axis is represented in Figure 2. The Zn and Si atoms are fully ordered, with large ZnO<sub>4</sub> tetrahedra pointing up and small SiO<sub>4</sub> tetrahedra pointing down.

The doped sample prepared by the same method used for the undoped one (referred to as method 1 or M1), with 12 h of total heating time, presents a BaZnSiO<sub>4</sub> X-ray pattern, Figure 1d, with low intensity and many extra lines. Some of them are pointed out in Figure 1 and are assigned to Ba<sub>2</sub>SiO<sub>4</sub> (3.01, 3.41, and 2.93 Å<sup>18a</sup>) and BaCO<sub>3</sub> (3.72 Å<sup>18b</sup>). In addition, this doped sample obtained by M1 has melted during the annealing. Therefore, the reaction from the doped silicates is not

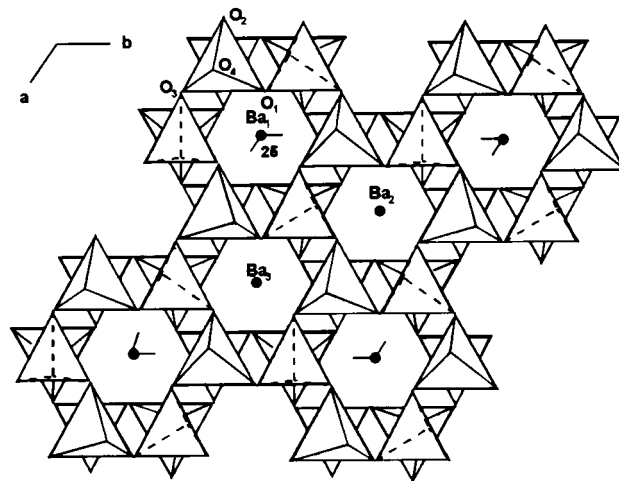


Figure 2. Structure of BaZnSiO<sub>4</sub> viewed along the *c* axis adapted from the structure of BaCoSiO<sub>4</sub> reported by Liu and Barbier.<sup>12</sup>

complete and the remaining low quantities of different components probably act as melting agents.

The BaZnSiO<sub>4</sub> doped sample prepared by method 2 (M2), even before the annealing, presents a X-ray

(18) Powder Diffraction File PDF-2 database sets 1-44. Pennsylvania Joint Committee on Powder Diffraction Standards-International Center for Diffraction Data. c 1988, PDG number (a) 26-1403 and (b) 44-1487. (CD-ROM).

(19) Huheey, J. B.; Keiter, E. A.; Keiter, R. L. *Inorganic Chemistry: Principles of Structure and Reactivity*. 4th ed.; Harper and Row Publishers: New York, 1993.

**Table 3.** IR Wavenumbers ( $\text{cm}^{-1}$ ) of Vibrational Modes Observed in the Spectra Presented in Figure 3 and Reported for Some Compounds in the Literature<sup>21–23</sup>

	$\text{SiO}_4^{4-}$ mode <sup>a</sup>				$\text{CO}_3^{2-}$ modes <sup>a</sup>				ref
	A <sub>1</sub> s ( $\nu_1$ )	F <sub>2</sub> s ( $\nu_3$ )	F <sub>2</sub> b ( $\nu_4$ )	E b ( $\nu_2$ )	CO <sub>2</sub> b ( $\nu_3$ )	CO <sub>2</sub> sym. s ( $\nu_1$ )	CO s ( $\nu_2$ )	CO <sub>2</sub> asym. s ( $\nu_4$ )	
MgCaSiO <sub>4</sub>	829	995, 965, 950, 890	595, 520	483					ref 21
Sr <sub>2</sub> SiO <sub>4</sub>	840	980, 964, 908, 892	528, 507						ref 21
Ba <sub>2</sub> SiO <sub>4</sub>	824	930, 903, 885	510, 492						ref 21
Ba <sub>2</sub> SiO <sub>4</sub>	815	976, 905, 847	510, 488		1448				Figure 3
Zn <sub>2</sub> SiO <sub>4</sub>		977, 934, 901, 865	610, 578	460					Figure 3
BaZnSiO <sub>4</sub>		916, 862	556, 503	406					Figure 3
BaCO <sub>3</sub>					1420		857	692	ref 22
BaCO <sub>3</sub>					1448	1056	855	690	Figure 3
SiO <sub>2</sub> modes									
	E s $\Delta\text{RSi-O}$	A <sub>2</sub> s $\Delta\text{RSi-O}$	E s $\Delta\text{RSi-O}$	E s $\Delta\text{RSi-O}$	E s b $\Delta\text{R Si-O}$ $\Delta\alpha\text{O-Si-O}$	E b $\Delta\alpha\text{O-Si-O}$	E b $\Delta\alpha\text{O-Si-O}$	ref 23	
$\alpha$ -cristobalite	1200	1140	1105	798	620	490	380	ref 23	
SiO <sub>2</sub>			1095	794	617	488	381	Figure 3	
ZnO lattice vibration									
ZnO					528, 495, 442				ref
									Figure 3

<sup>a</sup> s, stretching; b, bending.

diffraction pattern, Figure 1b,c, in good agreement with the undoped one, Figure 1a, indicating that it has the same structure represented in Figure 2. Thus, it seems that M2 is more useful than M1 to prepare doped BaZnSiO<sub>4</sub>. Besides, because the doped samples peak positions are similar to the undoped ones, it is clear that the Eu<sup>3+</sup> and Mn<sup>2+</sup> doping ions do not change the general structure. Maintenance of the structure is assumed on the basis of the calculations of the percentage difference between activators and matrix ion radii in the analyzed compounds (Table 2). An acceptable percentage difference in ion radius between doping and substituting ion must not exceed 30%. Data included in Table 2 suggest that in the case of BaZnSiO<sub>4</sub> there is a high probability of Eu<sup>3+</sup> replacing Ba<sup>2+</sup> despite their charge difference, and Mn<sup>2+</sup> probably substitutes for Zn<sup>2+</sup> ions. Neither activator ion is expected to occupy Si<sup>4+</sup> sites. The following explains the charge balance upon substitution of Ba<sup>2+</sup> by Eu<sup>3+</sup>. In M2, zinc oxide used as a precursor can lose oxygen during heating. In Zn<sub>1-x</sub>O, a nonstoichiometric system, the metal ion is easily reduced, mainly when  $x$  is very small,  $\approx 10^{-5}$ , or at high temperatures where the formation of defects is favored through entropy considerations.<sup>20</sup> Charge balance requires zinc atoms reduction to Zn<sup>+</sup> or Zn<sup>0</sup>. These reduced species formed during M2 can stabilize the Ba<sup>2+</sup>-Eu<sup>3+</sup> system. On the other hand, in M1, the precursor zinc orthosilicate doped with manganese probably does not provide Zn reduced species to charge compensate Eu<sup>3+</sup> substituted for Ba<sup>2+</sup>. This absence of balance can result in a less organized structure of the doped compound when compared with the undoped one, justifying the lower quality diffractogram pattern shown in Figure 1d.

**2. IR Spectroscopy.** Figure 3 shows the IR spectra of undoped precursors and a BaZnSiO<sub>4</sub> representative

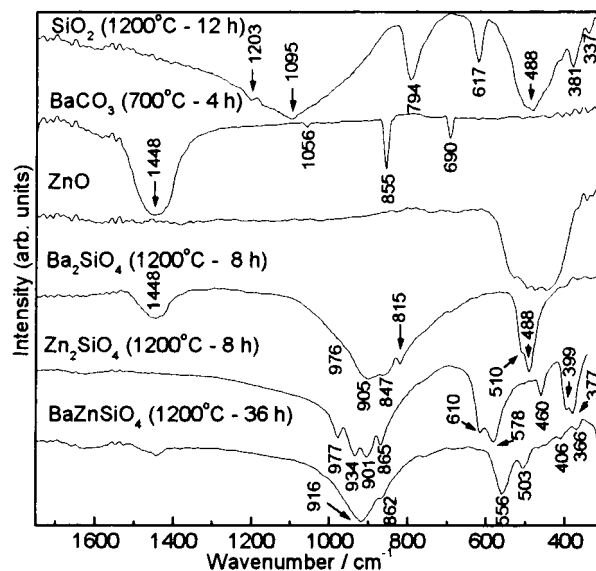


**Figure 3.** IR vibrational absorption spectra of BaZnSiO<sub>4</sub> precursors and a representative sample of this compound.

sample. Silica and barium carbonate standard precursors were heated in the specified conditions (see Figure 3) to supply crystalline samples. No specific literature data were found for BaZnSiO<sub>4</sub> IR spectra. To assign the observed vibrational modes, the BaZnSiO<sub>4</sub> spectra of different samples were compared with spectra of precursors and similar compounds in the literature,<sup>21</sup> whose IR wavenumbers of vibrational modes are listed in Table 3.

In orthosilicate structures, SiO<sub>4</sub><sup>4-</sup> complex anions are not linked but surrounded by Me<sup>2+</sup> cations and the

(21) Handke, M.; Urban, M. *J. Mol. Struct.* **1982**, *79*, 353.

(22) Gatehouse, B. M.; Livingstone, S. E.; Nyholm, R. S. *J. Chem. Soc.* **1958**, 3137.

(23) Ocaña, M.; Fornes, V.; Garcia Ramos, J. V.; Serna, C. J. *Phys. Chem. Miner.* **1987**, *14*, 527.

(20) Weller, M. T. *Inorganic Materials Chemistry*; Oxford Science Publications: Oxford, 1994.

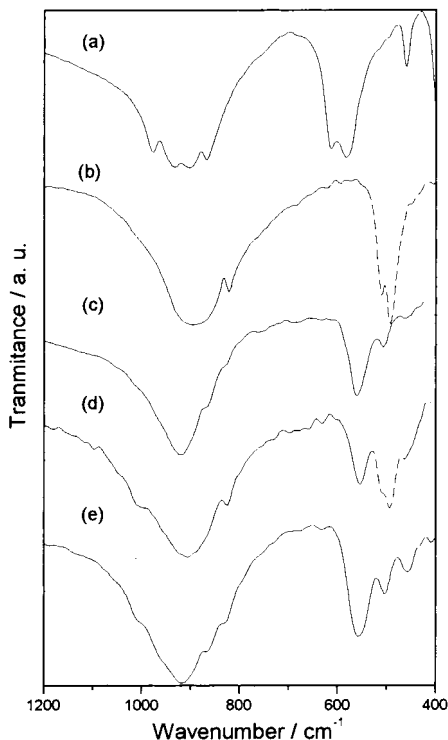


**Figure 4.** IR vibrational absorption spectra of (a)  $\text{Zn}_2\text{SiO}_4:\text{Mn}^{2+}$ , (b)  $\text{Ba}_2\text{SiO}_4:\text{Eu}^{3+}$ , (c)  $\text{BaZnSiO}_4$  undoped sample obtained after solid state reaction under  $1200^\circ\text{C}$  for 36 total heating hours, (d)  $\text{BaZnSiO}_4:\text{Eu}^{3+},\text{Mn}^{2+}$  sample obtained by M1 with 12 total heating hours, and (e)  $\text{BaZnSiO}_4:\text{Eu}^{3+},\text{Mn}^{2+}$  sample obtained by M2 with 24 total heating hours.

chemical bond distance between Si and O is shorter than the distance between Me and O. Therefore, internal modes for  $[\text{SiO}_4]$  are almost independent of external vibrations. In orthosilicate structures  $[\text{SiO}_4]$  internal modes are split because of their site symmetry (crystal field splitting) and unit-cell space symmetry (Davydov's splitting). Davydov's splitting depends on the anion-cation mixed vibrations whereas crystal field splitting depends on anion internal force field change.<sup>21</sup>

First, in Figure 3, some differences are observed between wavenumber positions of the standard precursors and all silicates. The vibrational modes attributed to Si–O stretching ( $\nu_3$ , in Table 3) in the silicate are shifted to smaller wavenumbers compared with silica, indicating the formation of  $\text{SiO}_4^{4-}$ . Second, the features and the splits present in the spectra of  $\text{Ba}_2\text{SiO}_4$  and  $\text{Zn}_2\text{SiO}_4$  related to  $\text{SiO}_4^{4-}$  modes are completely different. In addition, the  $\text{BaZnSiO}_4$  spectrum has its own identity. It can also be noted throughout Table 3 that the wavenumber positions related to  $\text{BaZnSiO}_4$  (hexagonal structure) and  $\text{MgCaSiO}_4$  (orthorhombic structure)  $\text{SiO}_4^{4-}$  modes are also different, exemplifying the sensibility of the technique in relation to the structure of the system. Finally, vibrational spectroscopy confirms the formation of silicate groups, which exhibits differences among the prepared silicates identified.

The sensitivity of the IR technique to a short distance structure of the systems makes possible a comparison of M1 and M2 (to prepare  $\text{BaZnSiO}_4$  doped samples). The  $1200\text{--}400\text{-cm}^{-1}$  IR spectra of doped silicate precursors compared with those of undoped  $\text{BaZnSiO}_4$  (36 h of total heating time) are shown in Figure 4. The large

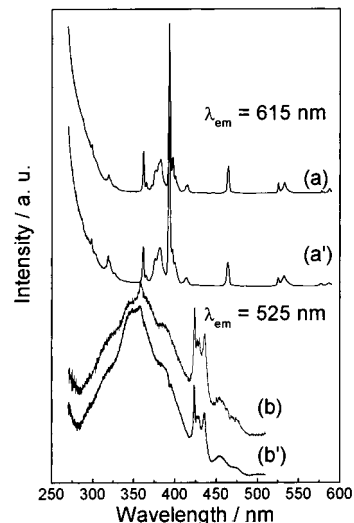


**Figure 5.** Excitation spectra at room temperature of  $\text{BaZnSiO}_4:\text{Eu}^{3+},\text{Mn}^{2+}$  obtained by M1 under 12 h of total heating (a,b) and by M2 under 24 h of total heating (a', b'). The emission wavelength fixed was 615 nm in (a) and (a') and 525 nm in (b) and (b').

band at  $1000\text{--}730\text{ cm}^{-1}$ , assigned to the  $\nu_3(\text{SiO}_4)$  mode in Table 3, is the same for doped (Figure 4d,e) and undoped (Figure 4c)  $\text{BaZnSiO}_4$  samples. On the other hand, the split band ranging from  $535$  to  $418\text{ cm}^{-1}$  (dashed line) assigned to the  $\nu_4(\text{SiO}_4)$  mode is observed in both  $\text{Ba}_2\text{SiO}_4:\text{Eu}^{3+}$  and doped  $\text{BaZnSiO}_4$  prepared by M1 (Figure 4b,d). This fact supports the conclusion based on X-ray diffraction that barium orthosilicate is also formed by M1.

**3. UV–Vis Luminescence Spectroscopy.** The excitation and emission spectra at room temperature of  $\text{BaZnSiO}_4:\text{Eu}^{3+},\text{Mn}^{2+}$  samples prepared by M1 and M2 are represented in Figures 5 and 6, respectively. In both cases, it is possible to observe the different optical transitions that are related to each activator depending on the wavelength chosen. The excitation spectra measured fixing the highest intensity of  ${}^5\text{D}_0 \rightarrow {}^7\text{F}_2$   $\text{Eu}^{3+}$  relaxation transition (615 nm) in Figure 5a,a' show the group of  $\text{Eu}^{3+}$  excitation transitions assigned to  ${}^7\text{F}_0 \rightarrow {}^5\text{L}_6, {}^5\text{D}_3$ . The corresponding emission spectra using the 393 nm excitation  ${}^7\text{F}_0 \rightarrow {}^5\text{L}_6$  transition, shown in Figure 6a,a', is a set of relaxation transitions  ${}^5\text{D}_0 \rightarrow {}^7\text{F}_{0,1,2,3,4}$  in the red region attributed to the  $\text{Eu}^{3+}$  in low-symmetry sites.<sup>24</sup> On the other hand, the excitation spectra represented in Figure 5b,b' show the set of transitions of tetrahedral  $\text{Mn}^{2+}$  ion,  ${}^6\text{A}_1 \rightarrow {}^4\text{T}_1$ ,  ${}^6\text{A}_1 \rightarrow {}^4\text{T}_2$ ,  ${}^6\text{A}_1 \rightarrow {}^4\text{E}$ ,  ${}^4\text{A}_1(4\text{G})$ ,  ${}^6\text{A}_1 \rightarrow {}^4\text{T}_2$ , and  ${}^6\text{A}_1 \rightarrow {}^4\text{E}(4\text{D})$ ,<sup>25</sup> and in the emission spectra, Figure 6b,b', a green broad band attributed to the  ${}^4\text{T}_1 \rightarrow {}^6\text{A}_1$   $\text{Mn}^{2+}$  transition is mainly observed. The weak emission line observed at the lower energy side in Figure 6b,b' at 615 nm is assigned to  ${}^5\text{D}_0 \rightarrow {}^7\text{F}_2$   $\text{Eu}^{3+}$  transition. The appearance of this  $\text{Eu}^{3+}$  emission is likely to support the belief that there is energy transfer from  $\text{Mn}^{2+}$  to  $\text{Eu}^{3+}$  because the 422 nm excitation wavelength is only observed in the  $\text{Mn}^{2+}$  excitation spectra,  ${}^6\text{A}_1 \rightarrow {}^4\text{E}$ ,  ${}^4\text{A}_1(4\text{G})$  transition. Finally, Figure 6c,c' shows that when the excitation wavelength

(24) Carnall, W. T.; Goodman, G. L.; Rajnak, K.; Rana, R. S. J. *Chem. Phys.* **1989**, *90*, 3443.

(25) Lever, A. B. P. *Inorganic Electronic Spectroscopy*, 2nd ed.; Elsevier: New York, 1984.

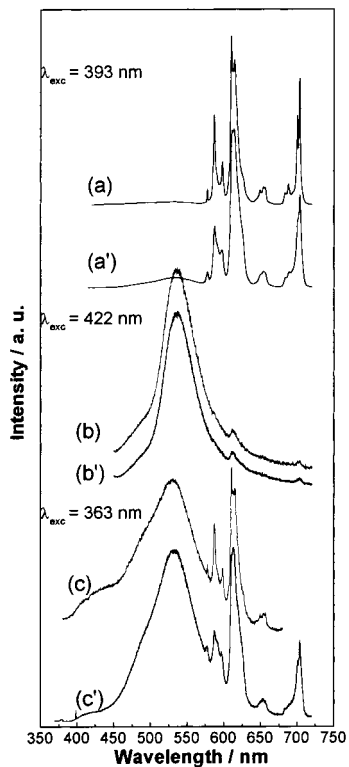


**Figure 6.** Emission spectra at room temperature of  $\text{BaZnSiO}_4:\text{Eu}^{3+},\text{Mn}^{2+}$  obtained by method 1 under 24 h of total heating (a,b,c) and by method 2 under 12 h of total heating (a',b',c'). The excitation wavelength fixed was 393 nm in (a) and (a'), 422 nm in (b) and (b'), and 363 nm in (c) and (c').

363 nm is used, it is possible to observe both  $\text{Eu}^{3+}$  and  $\text{Mn}^{2+}$  transitions recovering most of the visible spectrum due to simultaneous excitation of  $\text{Eu}^{3+}$  and  $\text{Mn}^{2+}$  ions.

On the basis of the results concerning room-temperature spectra of the doped samples, it seems that, despite the differences in XRD and IR data, the doped  $\text{BaZnSiO}_4$  samples obtained by methods M1 and M2 have almost the same optical excitation and emission behavior. Nevertheless, some measurements were carried out at low temperature (liquid  $\text{N}_2$ ), monitoring the  $^5\text{D}_0 \rightarrow ^7\text{F}_0$   $\text{Eu}^{3+}$  transition in each doped  $\text{BaZnSiO}_4$  sample, and some different features are observed (see Figure 7). Considering that in the  $\text{BaZnSiO}_4$  structure there are three different low-symmetry barium sites on which  $\text{Eu}^{3+}$  can substitute, the  $^5\text{D}_0 \rightarrow ^7\text{F}_0$  transition can consist of one more line. Therefore,  $\text{BaZnSiO}_4:\text{Eu}^{3+},\text{Mn}^{2+}$  prepared by M1 (Figure 7a) shows two lines centered on 577.6 and on 579.2 nm, one stronger and straighter and the other weaker and broader, respectively.  $\text{BaZnSiO}_4:\text{Eu}^{3+},\text{Mn}^{2+}$  prepared by M2, on the other hand, exhibits just one broad line with a maximum at 577.6 nm (Figure 7b). Two of the  $\text{Ba}^{2+}$  sites in the  $\text{BaZnSiO}_4$  host lattice have a CN of 9, but with different site symmetry (2a and 2b), so they are slightly different and cannot strongly modify the values of  $^5\text{D}_0$  or  $^7\text{F}_0$  levels. The third  $\text{Ba}^{2+}$  site with a CN of 6 and site symmetry 2b should result in a different position of the  $^5\text{D}_0 \rightarrow ^7\text{F}_0$  transition and must have low occupation probability. Then, in  $\text{BaZnSiO}_4:\text{Eu}^{3+},\text{Mn}^{2+}$  prepared by M2, the broad line observed can be resolved into at least two Lorentzian curves (dashed lines in Figure 7b), one weaker with a maximum at 576.6 and another stronger at  $\approx 577.7$  nm. The strongest line at 577.7 can

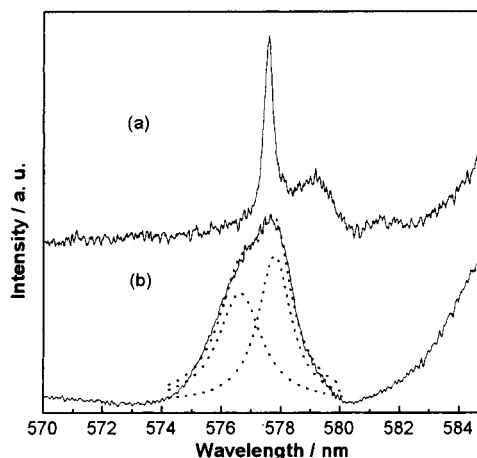


**Figure 7.** Emission spectra in the region of  $^5\text{D}_0 \rightarrow ^7\text{F}_0$   $\text{Eu}^{3+}$  transition at  $\text{N}_2$  liquid temperature of  $\text{BaZnSiO}_4:\text{Eu}^{3+},\text{Mn}^{2+}$  obtained by method 1 under 12 h of total heating (a) and by method 2 under 24 h of total heating (b). The excitation wavelength fixed was 393 nm in both cases.

be assigned to  $\text{Eu}^{3+}$  in the  $\text{Ba}^{2+}$  site with a CN of 9 and the other to  $\text{Eu}^{3+}$  in the  $\text{Ba}^{2+}$  site with a CN of 6. In the case of  $\text{BaZnSiO}_4:\text{Eu}^{3+},\text{Mn}^{2+}$  prepared by M1 where the  $\text{Ba}_2\text{SiO}_4$  phase is detected by XRD and IR,  $\text{Eu}^{3+}$  can also substitute for  $\text{Ba}^{2+}$  in this compound, which explains the shifted broad weak line presented in the emission spectra at 579.2 nm (Figure 7a). The other line, at 577.6 nm, is located at the same position as that for the sample prepared by M2 and can have analogous assignment on  $\text{Eu}^{3+}$  in the  $\text{Ba}^{2+}$  site with a CN of 9. The  $\text{Ba}^{2+}$  site with a CN of 6 probably does not have a large occupation.

In our discussion of the X-ray diffraction data it is proposed that the  $\text{Zn}^{2+}$  species can charge compensate  $\text{Eu}^{3+}$  substituted for  $\text{Ba}^{2+}$ . Spectroscopy studies of the  $\text{Ba}_2\text{SiO}_4:\text{Eu}^{3+}$  compound was reported<sup>7</sup> and the evidence of  $\text{Eu}^{3+}-\text{O}^{2-}$  associates in this system as a result of a charge-compensating mechanism was established. This  $\text{Eu}^{3+}-\text{O}^{2-}$  associates presented a  $^5\text{D}_0 \rightarrow ^7\text{F}_0$   $\text{Eu}^{3+}$  transition and charge-transfer band at the unusual positions of 572 and 340 nm, respectively, while the  $\text{Eu}^{3+}$  in  $\text{Ba}^{2+}$  sites showed a  $^5\text{D}_0 \rightarrow ^7\text{F}_0$   $\text{Eu}^{3+}$  transition at a standard position of 581 nm. Therefore, a charge compensation mechanism can also be inferred in the  $\text{BaZnSiO}_4:\text{Eu}^{3+},\text{Mn}^{2+}$  system by assuming the formation of  $\text{Eu}^{3+}-\text{O}^{2-}$  associates. Extra spectroscopic measurements were also performed for all  $\text{BaZnSiO}_4:\text{Eu}^{3+},\text{Mn}^{2+}$  systems by fixing appropriate wavelengths to identify the presence of  $\text{Eu}^{3+}-\text{O}^{2-}$  associates. But no evidence is found in the excitation and emission spectra measured, indicating that in  $\text{BaZnSiO}_4:\text{Eu}^{3+},\text{Mn}^{2+}$  systems  $\text{Eu}^{3+}-\text{O}^{2-}$  associates are not formed. These results support the hypothesis that charge is compensated by  $\text{Zn}^{2+}$  species.

Lifetime measurements were carried out by monitoring  $\text{Eu}^{3+}$  and  $\text{Mn}^{2+}$  transitions in the silicate precursors as well as in the barium and zinc orthosilicate systems prepared by M1 and M2. These results are summarized in Table 4. A significant decrease of the lifetime for the  $\text{Mn}^{2+}$  ion radiative level transition in M1 and M2 barium and zinc orthosilicates is observed when compared to that of the zinc orthosilicate precursor. This lifetime decrease, approximately to half the value, is probably related to energy transfer mechanisms between  $\text{Mn}^{2+}$  and  $\text{Eu}^{3+}$  discussed above.

**Table 4. Lifetime Values of Doped Compounds**

compound	$\lambda$ position/nm		ion monitored	$\tau$ /ms
	excitation	emission		
BaZnSiO <sub>4</sub> :Eu <sup>3+</sup> ,Mn <sup>2+</sup> (M1)	393	615	Eu <sup>3+</sup>	1.94
	424	536	Mn <sup>2+</sup>	4.50
BaZnSiO <sub>4</sub> :Eu <sup>3+</sup> ,Mn <sup>2+</sup> (M2)	394	615	Eu <sup>3+</sup>	1.78
	424	530	Mn <sup>2+</sup>	4.52
Ba <sub>2</sub> SiO <sub>4</sub> :Eu <sup>3+</sup>	394	612	Eu <sup>3+</sup>	1.98
Zn <sub>2</sub> SiO <sub>4</sub> :Mn <sup>2+</sup>	422	525	Mn <sup>2+</sup>	10.2

**Table 5. C.I.E. Chromaticity Coordinate, xy**

compound	chromaticity coordinates		$\lambda_{\text{exc}}$ /nm	ref
	x	y		
BaZnSiO <sub>4</sub> :Eu <sup>3+</sup> ,Mn <sup>2+</sup> (M2)	0.348	0.474	363	this work
Ba <sub>2</sub> SiO <sub>4</sub> :Eu <sup>3+</sup>	0.234	0.248	340	this work
Zn <sub>2</sub> SiO <sub>4</sub> :Mn <sup>2+</sup>	0.243	0.693	365	this work
Zn <sub>2</sub> SiO <sub>4</sub> :Mn <sup>2+</sup>	0.252	0.691		ref 2
400-W HPMV Lamp	0.311	0.391		ref 2

To evaluate the material performance on color luminescent emission, C.I.E., chromaticity coordinates  $xy$  were obtained from calculations based on the emission spectra. The data are summarized in Table 5. Only BaZnSiO<sub>4</sub>:Eu<sup>3+</sup>,Mn<sup>2+</sup> (M2) was chosen to be investigated due to the fact that this sample presents the best structural and optical characteristics. The C.I.E. calculated values for precursors Ba<sub>2</sub>SiO<sub>4</sub>:Eu<sup>3+</sup> and Zn<sub>2</sub>SiO<sub>4</sub>:Mn<sup>2+</sup> and some values reported in the literature<sup>3</sup> for Zn<sub>2</sub>SiO<sub>4</sub>:Mn<sup>2+</sup> and a 400-W HPMV lamp are also included. The silicate doped with both Eu<sup>3+</sup> and Mn<sup>2+</sup> presents  $xy$  C.I.E. chromaticity coordinates related to the emission color with green and red components, resulting in a color emission close to white.

### Conclusions

The present paper reported on BaZnSiO<sub>4</sub> activated by Eu<sup>3+</sup> and Mn<sup>2+</sup> studies, where Eu<sup>3+</sup> substitutes for

Ba<sup>2+</sup> and Mn<sup>2+</sup> substitutes for Zn<sup>2+</sup> ions. X-ray and IR results indicate that the BaZnSiO<sub>4</sub> undoped sample is successfully obtained using the method started from Ba<sub>2</sub>SiO<sub>4</sub> and Zn<sub>2</sub>SiO<sub>4</sub> independently prepared. On the other hand, doped BaZnSiO<sub>4</sub> started from the mixture containing the oxides, carbonates, and the activators presents a larger purity phase. Zinc oxide precursors appear to help charge compensation by the formation of reduced species.

Luminescence studies on doped samples resulted in the observation of different optical transitions that are related to each activator in the BaZnSiO<sub>4</sub> matrix. Energy transfer from Mn<sup>2+</sup> to Eu<sup>3+</sup> ions is also observed. When the excitation wavelength 363 nm is used, both Eu<sup>3+</sup> and Mn<sup>2+</sup> transitions covering most of the part of the visible spectrum are detected. Because in fluorescent high-pressure mercury vapor lamps the radiation originated by the mercury ion is 366 nm, it is possible to suggest that BaZnSiO<sub>4</sub>:Eu<sup>3+</sup>,Mn<sup>2+</sup> has some adequate luminescent features that suggest its use as a lamp applied material.

**Acknowledgment.** This work was financially supported by FAPESP and CNPq. A.M.P. thanks CNPq for the scholarship. The authors also gratefully acknowledge to Dr. Alain Garcia and Prof. Claude Fouassier (Researcher and Research Director of CNRS, ICMCB, France, respectively) for providing the possibility to perform color chromaticity measurements and to Solange Aranha for English review.

CM000063G